Available online at www.sciencedirect.com
SCIENCE DIRECT®
Journal of Solid State Chemistry 177 (2004) 2998–3006
JOURNAL OF SOLID STATE CHEMISTRY
http://elsevier.com/locate/jssc

Thermoelectric properties and antiferromagnetism of the new ternary transition metal telluride $CrAuTe_4$

Thomas K. Reynolds,[a] Michael A. McGuire,[b] and Francis J. DiSalvo[a,*]

[a] *Department of Chemistry and Chemical Biology, Baker Laboratory, Cornell University, Ithaca, NY 14853, USA*
[b] *Department of Physics, Clark Hall, Cornell University, Ithaca, NY 14853, USA*

Received 13 November 2003; received in revised form 9 April 2004; accepted 18 April 2004

Available online 24 June 2004

Abstract

The new ternary transition metal telluride $CrAuTe_4$ has been discovered through solid-state reaction of the elements. The crystal structure is solved in the monoclinic space group $P2/m$ (No. 10) with lattice parameters $a = 5.4774(7)$ Å, $b = 4.0169(6)$ Å, $c = 7.3692(13)$ Å, and $\beta = 90.604(10)^\circ$. The structure is related to that of the binary compound $AuTe_2$, and a derivation of the structure of $CrAuTe_4$ from $AuTe_2$ is shown. Measurements of the thermopower, thermal conductivity, electrical resistivity, and magnetic susceptibility are presented. The compound undergoes a paramagnetic to antiferromagnetic transition at 255 K.

Keywords: Thermoelectric; Antiferromagnetism; Chromium–gold telluride

1. Introduction

Most of the best thermoelectric materials known to date contain heavy elements. Perhaps one of the largest areas of research in thermoelectric materials is focused on chalcogenide (the elements S, Se, and Te) compounds. In particular, compounds of Se and Te have been extensively studied, since sulfides generally have larger bandgaps and relatively high-thermal conductivity, which are undesirable features for thermoelectrics. Most of the initial research in these materials following the discovery of the good thermoelectric behavior of Bi_2Te_3 was focused on forming solid solutions of Bi_2Te_3 with other chalcogenides [1–8]. Indeed, the best thermoelectric for use near room temperature to date is an alloy of Bi_2Te_3 and Sb_2Te_3.

The potential utility of a material for thermoelectric applications is determined by the dimensionless figure of merit ZT, where $ZT = S^2T/\rho\kappa$. In this equation, S is the Seebeck coefficient or thermopower, ρ is the electrical resistivity, κ is the thermal conductivity, and T is temperature. At room temperature, the best materials have a ZT near 1. A ZT of 3 or 4 would enable devices that could compete with the efficiency of a home compressor-based refrigerator [9].

Since heavy-metal chalcogenides seem to be one of the most promising areas for thermoelectrics research, we have begun to examine heavy-metal telluride systems which have been little studied. In particular, very few ternary and no quaternary gold tellurides are known. In fact, the only known ternary gold tellurides are Ag_3AuTe_2 [10], $AgAuTe_4$ [11], and $MAuTe$ [12] (where M = Na, K, Rb, or Cs). Our study of TM/Au/Te (TM = transition metal) systems produced the new phase $CrAuTe_4$. In this compound, a direct single bond between some of the Te atoms forms Te_2 pairs, thus formal oxidation states can be assigned as: $Cr^{3+}Au^{3+}(Te_2)^{2-}Te_2^{2-}$. We have measured the thermopower, thermal conductivity, electrical resistivity, and magnetic susceptibility of this compound and herein present those results along with the crystal structure.

2. Experimental

2.1. Reagents

All reagents were used as received: Chromium powder, 99.9% purity, −100 mesh, United Mineral

*Corresponding author. Fax: +1-607-255-4137.
E-mail address: fjd3@cornell.edu (F.J. DiSalvo).

0022-4596/$ - see front matter © 2004 Elsevier Inc. All rights reserved.
doi:10.1016/j.jssc.2004.04.029

and Chemical Corp.; Gold metal splatters, 99.999% purity, Cerac Inc.; Tellurium powder, 99.99% purity, −30 mesh, Cerac Inc.

2.2. Synthesis

$CrAuTe_4$ was initially synthesized directly by the combination of Cr, Au, and Te in a 2:2:7 ratio (equivalent to $Cr_2Te_3 + 2AuTe_2$, which is on the tie-line between two of the known binaries: Cr_2Te_3 and $AuTe_2$). The reactants were loaded into a silica tube and sealed under vacuum to prevent reaction of the elements with the air. The silica tube was then placed vertically in a box furnace and heated over 9 h to 900°C and held there for 2 days. The reaction mixture was then slow cooled to 300°C over 6 days, and then allowed to cool to room temperature with the furnace power off. The reaction product was a dark black and silver mass with large black, rod-like crystals protruding from the surface.

Standardless energy-dispersive electron microprobe analysis (JEOL 8900R) was performed on several of the rod-shaped crystals. The results confirmed that the sample contained Cr, Au and Te in ratios consistent with the stoichiometry $CrAuTe_4$ and no other elements with $Z > 10$. Crystal structure determination then confirmed that this was the correct stoichiometry.

The compound was then able to be prepared phase pure by a stoichiometric reaction of the elements. Cr, Au, and Te were weighed out in a 1:1:4 ratio and sealed in a silica tube under vacuum. After heating to 900°C over 9 h, the reaction mixture was held at this temperature for 2 days and then slow cooled to 500°C over 4 days. The furnace power was then turned off and the sample was allowed to cool to room temperature. The resulting powder was then ground and pressed into a pellet (approximate size: $\frac{1}{2}''$ diameter, $\frac{1}{4}''$ long) in a hardened steel die. This pellet was sealed in a silica tube and heated to 500°C over 5 h and held at this temperature for 2 days. The furnace was then turned off, and the pellet was examined. The pellet had deformed, suggesting partial melting, and rod-like crystals could be seen growing from the surface. The mixture was again ground and pressed into a pellet. The pellet was sealed in a silica tube and heated to 400°C over 4 h and held at this temperature for 2 days. The sample was cooled to room temperature with the furnace power off. The pellet maintained its shape and the resulting product was phase pure by powder X-ray diffraction. To prepare this compound for properties measurement, this powder was again pressed into a pellet and heated to 400°C over 4 h. The reaction was then held at this temperature for 11 days to promote sintering and grain growth.

The crystals and polycrystalline powder produced by the above reactions are not sensitive to moisture or oxygen. The pellet obtained by the latter reaction is silver in color, and the metallic luster is maintained in air indefinitely.

2.3. Single crystal X-ray diffraction

A black, regularly shaped rod-like crystal of size 0.20 mm × 0.08 mm × 0.02 mm was mechanically selected from the polycrystalline reaction mass. The crystal was mounted in poly(butenes) oil (viscosity at 99°C 109–125 cst, $d = 0.88$–0.89, Catalogue # 38,868-8, Aldrich) and bathed in a cold nitrogen stream for data collection at 166 K. A Bruker SMART CCD diffractometer equipped with a 1 K CCD detector and a 3 kW sealed tube molybdenum X-ray source was used for the data collection. The program SMART was used to collect the data and the program SAINT was used to integrate the data and refine the unit cell parameters based on all strong reflections [13]. Four different ω scans were collected ($\phi = 0°$, 120°, 240°, and 180°). 606 frames of the first ϕ angle were taken, and 400 frames were taken for the additional ϕ angles. The collection time for each frame was 30 s. The width of these scans, $\Delta\omega$, was 0.3° for each frame.

Since the crystal contains heavy elements, an absorption correction was applied using the program X-Shape [14]. This program optimizes the crystal shape based on equivalent reflections and then a pseudo face-indexed absorption correction can be applied based on this optimized crystal shape.

The determination of the space group was carried out using the program X-PREP from the SHELXTL program suite provided with the Bruker instrumentation [15,16]. The solution of the crystal structure was obtained by using the program SIR92 [17] and was refined using SHELXL97 with the WingX program suite [18].

X-PREP suggested three possible space groups for the crystal structure. The three possibilities given were $P2_1$, Pm, and $P2/m$. A solution was found in the highest symmetry space group, $P2/m$. The initial structure solution from SIR92 contained 1 Au, 1 Cr, and 2 Te atoms in the asymmetric unit. After the initial refinement with SHELXL97, R_1 was 4.29% and wR_2 was 13.25%, indicating that the initial model was essentially complete. All of the atoms showed appropriate thermal parameters, and there were no spurious peaks in the Fourier difference map. SHELXL97 suggested that an extinction correction was necessary, and after refining, R_1 decreased to 3.61% and wR_2 decreased to 12.50%. The thermal parameters were then refined anisotropically to give a R_1 of 2.96% and a wR_2 of 10.22%. After using the suggested weights given in SHELXL97, the final R_1 was 2.66% and wR_2 was 6.72%. The goodness-of-fit of the data was 1.105. The highest peak in the Fourier difference map was 2.28 eÅ^{-3} (0.66 Å from Au) and the lowest valley was −2.15 eÅ^{-3} (0.89 Å from Au).

Electron density differences close to heavy atoms such as Au are usually ascribed to data truncation. Here, data was collected only for $2\theta < 72.56°$.

Table 1
Single crystal refinement data for $CrAuTe_4$

Empirical formula	$CrAuTe_4$
Formula weight	759.37 g/mol
Temperature	166 K
Wavelength	0.71073 Å
Crystal system	Monoclinic
Space group	$P2/m$
Unit cell dimensions	$a = 5.4774(7)$ Å
	$b = 4.0169(6)$ Å $\beta = 90.604(10)°$
	$c = 7.3692(13)$ Å
Volume	162.13(4) Å^3
Color	Black
Z	1
Calculated density	7.777 Mg/m^3
Absorption coefficient	41.769 mm^{-1}
$F(000)$	311
Crystal size	$0.20 \times 0.08 \times 0.02$ mm^3
θ range	2.76°–36.28°
Limiting indices	$-9 \leqslant h \leqslant 8$
	$-6 \leqslant k \leqslant 5$
	$-10 \leqslant l \leqslant 10$
Reflections collected/unique	2010/690 [R(int) = 0.0601]
Completeness to $\theta = 36.28°$	78.6%
Refinement method	Full-matrix least squares on F^2
Data/restraints/parameters	690/0/22
Goodness-of-fit on F^2	1.105
Final R indices ($I > 2\sigma(I)$)[a,b]	$R_1 = 0.0266$, $wR_2 = 0.0672$
R indices (all data)[a,b]	$R_1 = 0.0271$, $wR_2 = 0.0674$
Extinction coefficient	0.0166(17)
Largest diff. peak and hole	2.282 and −2.150 eÅ^{-3}

[a] $R_1 = \sum||F_o| - |F_c||/\sum|F_o|$
[b] $wR_2 = [\sum w(F_o^2 - F_c^2)^2/\sum w(F_o^2)^2]^{1/2}$. $w^{-1} = [\sigma(F_o^2) + (aP)^2 + bP]$ where $P = [\max(F_o^2, 0) + 2F_c^2]/3$.

Table 2
Atomic coordinates and equivalent isotropic displacement parameters (Å^2) for $CrAuTe_4$

Atom	x	y	z	U_{eq}
Au	0.0000	0.0000	0.0000	0.00781(14)
Cr	0.0000	0.5000	0.5000	0.0063(3)
Te(1)	0.22779(9)	0.5000	0.83042(7)	0.00754(14)
Te(2)	0.70069(8)	0.0000	0.62284(7)	0.00756(14)

U_{eq} is defined as one-third of the trace of the orthogonalized U_{ij} tensor.

A summary of the crystal structure refinement data is shown in Table 1. A list of the atomic positions and isotropic thermal parameters are given in Table 2. The anisotropic thermal parameters are given in Table 3. Selected bond lengths and angles are listed in Tables 4 and 5.

2.4. Transport property measurements

Since the compound produced was silver/black in color, transport property measurements were carried out on a polycrystalline pellet. The pressed pellet, which had been annealed for 11 days to promote sintering and grain growth, was cut into a rectangular parallelepiped

Table 4
Selected bond lengths (Å) for $CrAuTe_4$

Bond	Length (Å)
Au–Te(1)	2.6805(4) (×4)
Au–Te(2)	3.2120(7) (×2)
Cr–Te(1)	2.7243(7) (×2)
Cr–Te(2)	2.7518(4) (×4)
Te(2)–Te(2)	2.8332(10)

Table 5
Selected bond angles (°) for $CrAuTe_4$

Angle	Angle (°)
Te(1)–Au–Te(1)	97.06(2)
Te(1)–Au–Te(1)	82.94(2)
Te(1)–Au–Te(1)	180.00(2)
Te(1)–Au–Te(2)	80.354(15)
Te(1)–Au–Te(2)	99.646(15)
Te(2)–Au–Te(2)	180.0
Te(1)–Cr–Te(1)	180.0
Te(1)–Cr–Te(2)	91.442(15)
Te(1)–Cr–Te(2)	88.558(15)
Te(2)–Cr–Te(2)	93.751(19)
Te(2)–Cr–Te(2)	86.249(19)
Te(2)–Cr–Te(2)	180.0
Au–Te(1)–Au	97.06(2)
Au–Te(1)–Cr	101.867(15)
Cr–Te(2)–Cr	93.751(19)
Cr–Te(2)–Te(2)	104.52(2)
Cr–Te(2)–Au	89.095(14)
Te(2)–Te(2)–Au	159.80(3)

Table 3
The anisotropic displacement parameters (Å^2) for the compound $CrAuTe_4$

Atom	U_{11}	U_{22}	U_{33}	U_{23}	U_{13}	U_{12}
Au	0.00971(18)	0.00636(18)	0.0074(2)	0.000	0.00073(13)	0.000
Cr	0.0051(6)	0.0063(6)	0.0073(8)	0.000	−0.0017(5)	0.000
Te(1)	0.0079(2)	0.0069(2)	0.0079(3)	0.000	0.00012(15)	0.000
Te(2)	0.00618(19)	0.0073(2)	0.0092(3)	0.000	0.00037(15)	0.000

The exponent of the anisotropic displacement factor has the following form: $-2\pi^2(h^2a^{*2}U_{11} + \cdots + 2hka^*b^*U_{12})$.

of dimensions 0.355 cm × 0.460 cm × 0.860 cm with a diamond wheel saw for measurements of the Seebeck coefficient, thermal conductivity, and electrical resistivity. The Seebeck coefficient and thermal conductivity were measured simultaneously, while electrical resistivity was measured during a separate run. All of the measurements were made on the same sample to ensure that they reflect only one doping state of the material.

Measurements were carried out in a home-built apparatus designed to measure these properties from liquid helium temperature up to room temperature. The probe is made to fit into a liquid helium storage dewar, and the sample stage inside the probe has a weak thermal link to this environment. A heater cartridge within the sample stage is used to control the base temperature of the sample. Both ends of the sample are wet with indium metal to insure good electrical and thermal contact between the thermocouples, heater, and sample. 40 AWG Au(0.07% Fe)/Chromel-P thermocouples are soldered with indium to each end of the sample to measure the temperature difference between the ends. At the same time, the Chromel-P wires are used to measure the voltage difference across the sample. This insures that the temperature measurements and the voltage measurements occur at the same positions. Indium is used to solder a 6 kΩ resistor ($\frac{1}{4}$ W) wrapped with copper foil to one end of the sample to serve as a resistive heater. The other end of the sample is soldered with indium to a removable copper screw which attaches to the sample stage to act as a heat sink.

For reliable thermal conductivity measurements, heat loss from the resistor through paths other than the sample should be minimized. Thus, the sample is maintained in a vacuum of 10^{-5} Torr or less so that heat losses to the surrounding gas are minimized. A copper radiation shield is placed around the sample to reduce radiative heat loss.

For each data point, a computer-controlled temperature controller (Cryocon Model 32) is used to stabilize the base temperature of the sample. Typical stability for the sample stage is ±10 mK. The sample heater is then turned on to a predetermined power setting to establish a temperature difference. Typically, the target temperature difference between the two ends is 4–5 K. While the sample is coming to equilibrium, temperature and voltage differences between the ends of the sample are measured at a rate of about two to three data points per second. This produces a roughly exponential curve of ΔT versus time. This curve is then fit to obtain the value of ΔT *if the sample were allowed to reach the steady state*. This extracted ΔT value can be obtained in several thermal time constants (typically as little as 30–40 s depending on the thermal conductivity of the sample), and agrees well with values obtained when the sample is allowed to reach true steady state. The sample heater is then turned off. While the sample is cooling, the sample voltage and the roughly exponential decay of ΔT with time are again monitored. The cooling ΔT curve is then fit in a similar manner to the heating curve, and a zero point offset is obtained for ΔT. The zero point offsets are small (on the order of a few hundredths of a Kelvin) and due to slight differences in the thermocouple wires. The differences in the two extrapolated ΔT values along with the measured power applied to the heater and sample dimensions are used to determine the thermal conductivity of the sample. This value is corrected for heat losses through the wires connected to the sample, which was determined in a separate experiment.

The slope from a linear fit of V versus ΔT gives the uncorrected thermopower. Since the voltage contacts are made with Chromel-P wires, the Seebeck coefficient for these wires must be subtracted from the measurements to find the Seebeck coefficient of the sample. The Seebeck coefficients obtained from the heating and cooling curves are then averaged to give a final value for the Seebeck coefficient.

To ensure that this technique is accurate, data points are taken at the beginning and end of the run using the steady-state method [19]. The values for Seebeck coefficient and thermal conductivity obtained by the two methods agree to within 3%. This technique was validated by using known Seebeck coefficient and thermal conductivity standards (Bi_2Te_3 obtained from Marlow Industries). The accuracy of the Seebeck coefficient is estimated to be ±5%. The accuracy of the thermal conductivity measurements is ±10%, and a large part of this error is due to measurement of the sample dimensions. Using this method, a high density of data points can be obtained in a much shorter time than when using the steady-state technique.

This same pellet was then mounted for electrical resistivity measurements using a standard four-point AC technique. Four spring-loaded gold pins (Ostby-Barton brand) were used to make pressure contacts to the sample. The distance between the two voltage contacts is 0.157 cm. The sample was checked to make sure the contacts were ohmic (i.e. the I–V curve is linear over several orders of magnitude). The same probe used for measuring Seebeck coefficient and thermal conductivity also is used for measuring resistivity, and temperature control is identical. For this measurement, however, high vacuum is not necessary. Measurements of sample resistance are taken with a Linear Research LR-700 AC resistance bridge. The frequency of the AC current is 16 Hz. At each data point, the temperature is stabilized and five resistance measurements are made and averaged. After multiplying by the geometrical factor, a value for resistivity at that temperature is obtained. The program then directs the temperature controller to another temperature and the process is repeated. Absolute errors in measurement of resistance as

determined from a NIST traceable platinum standard are very small, typically less than 1%. However, due to uncertainty in the measurement of the sample dimensions and distance between the voltage probes, the absolute error on the resistivity measurement is estimated to be on the order of 10%.

2.5. Magnetic property measurements

Magnetic susceptibility data were collected in the temperature range 5–300 K using a Quantum Design SQUID magnetometer. A polycrystalline sample cut from the same pellet used for transport property measurements was used for magnetic measurements. This sample was loaded into a gelatin capsule and had a weight of 217.7 mg. Data were collected in DC mode using a field of 50,000 Oe. An empty gelatin capsule was measured under the same conditions to determine its diamagnetic contribution to be subtracted from the measurement.

3. Results and discussion

3.1. Crystal structure description

The crystal structure and bonding in $CrAuTe_4$ are truly three dimensional. However, the crystal structure can be broken down into simpler pieces that are joined together to form the total crystal structure. A view down the *a*-axis, shown in Fig. 1, shows a layer that is composed of both Cr and Au bonded to Te. Cr is in octahedral coordination by Te, whereas Au is in square planar coordination by Te. The Au polyhedra form one-dimensional infinite square planar chains by sharing edges along the *b*-axis. Joined to these one-dimensional chains are a second set of one-dimensional chains with Cr-centered octahedra that also share edges. A layer is thus formed in the *yz* plane from the alternating sets of one-dimensional chains of Au and Cr polyhedra.

These layers are then stacked along the *a*-axis. The layer stacking geometry is evident in a view parallel to the *b*-axis as shown in Fig. 2. The layers shown in Fig. 1 are now perpendicular to the page (the *xz* plane). The layers are bonded to each other through Te–Te bonds that join $CrTe_6$ octahedra. These are close to Te–Te single bonds which have a bond length of 2.83 Å. The Te–Te bond length in elemental Te is 2.82 Å [20]. Also, the Te–Te dimer found in K_2Te_2 has a bond length of 2.86 Å [21]. Four of the six octahedral vertices around the Cr atom are bonded to these Te_2 dimers, which then bond to another Cr atom in the adjoining layer. The other two vertices of the octahedron around Cr bond to Au within the layer. In this manner, a three-dimensional structure is formed.

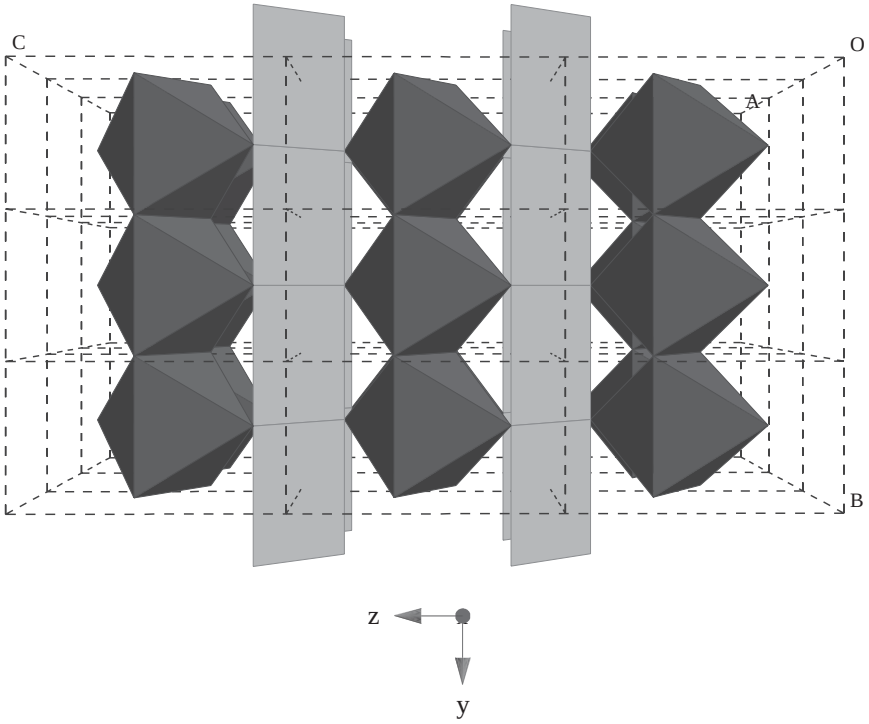

Fig. 1. Crystal structure of $CrAuTe_4$ viewed down the *a*-axis. Layers of alternating one-dimensional Au and Cr-centered polyhedral chains which run along the *b*-axis are apparent in the *yz* plane. The Au atoms are at the center of square planar Te anions and the Cr atoms are at the center of Te octahedra.

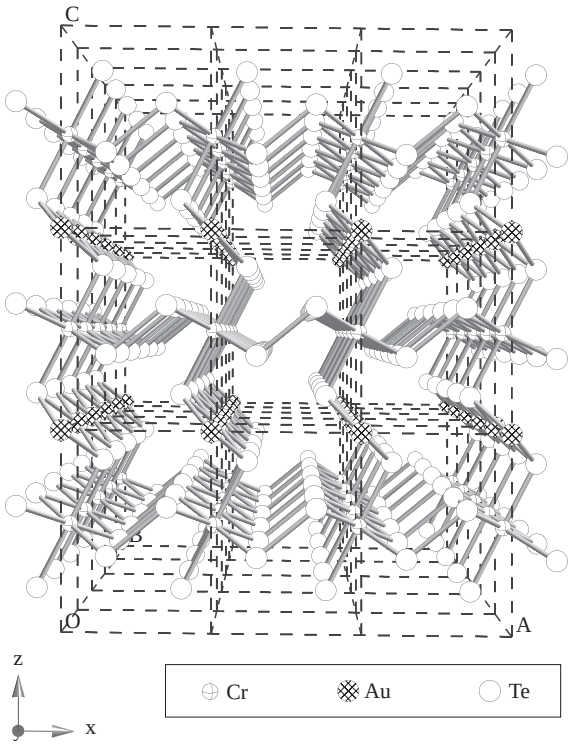

Fig. 2. Crystal structure of $CrAuTe_4$ viewed down the *b*-axis. The layers from Fig. 1 are now viewed edge on, and the connectivity of these layers to each other is through a Te–Te single bond.

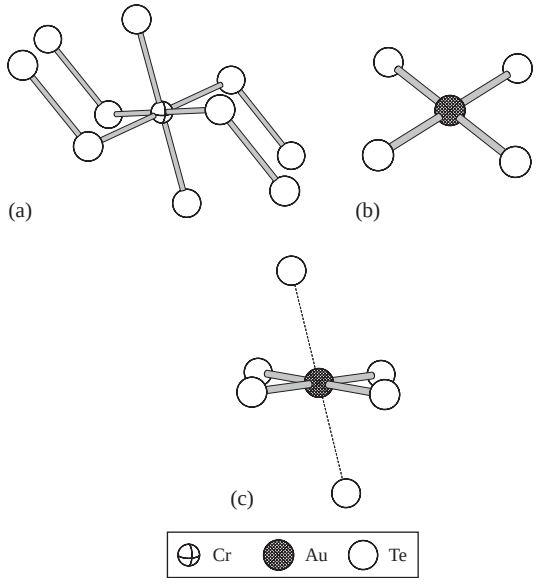

Fig. 3. Bonding environment of the Cr and Au atoms in $CrAuTe_4$. (a) Cr, (b) Au, and (c) Au showing the second-closest contacts with Te form an elongated, distorted octahedron.

A representation of the bonding environments for Cr and Au are shown in Fig. 3.

The structure of $CrAuTe_4$ is related to that of $AuTe_2$. In $AuTe_2$, there are two short Au–Te bonds (2.67 Å), and four long Au–Te bonds (2.98 Å) [22]. The four longer Au–Te bonds are much shorter than a van der Waals contact (3.72 Å), but decidedly much longer than a single Au–Te bond. These four longer contacts are in a square planar arrangement around the Au atom. In $AuTe_2$, layers similar to those in $CrAuTe_4$ are found, but the coordination environments are different. Instead of having alternating Cr and Au polyhedra, only Au polyhedra with two short and four long contacts forming a distorted octahedron are formed. To transform these layers into those found in $CrAuTe_4$, the four long Au–Te bonds are shortened to a normal single bond Au–Te distance (2.68 Å), and the two short Au–Te bonds are elongated to 3.21 Å. This gives square planar Au. The Au atom next to this square planar Au is replaced with a Cr atom, and the layer shown in Fig. 1 results. A representation of the transformation between these two structures is shown in Fig. 4.

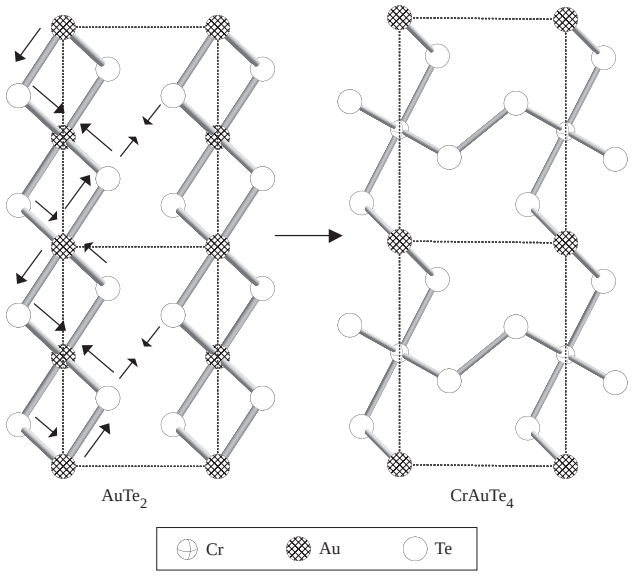

Fig. 4. Derivation of the $CrAuTe_4$ structure from the $AuTe_2$ structure. The arrows represent lengthening or shortening of bonds. Connectivity between the layers occurs in $CrAuTe_4$ through a Te–Te bond that is not present in $AuTe_2$.

3.2. Transport properties

Fig. 5 shows the thermopower of $CrAuTe_4$ as a function of temperature. A maximum thermopower of 55 μV/K occurs at 300 K. The sigmoidal shape of the curve is unusual, but the values of S tend towards zero as the temperature goes to zero, as demanded by thermodynamics. The resistivity of $CrAuTe_4$ is shown in Fig. 6. At 300 K the resistivity is 850 $\mu\Omega \cdot$ cm. The shape of the resistivity and thermopower curves are similar, which is true for many materials. As the resistivity decreases, the thermopower often also decreases. The value of the resistivity at room temperature

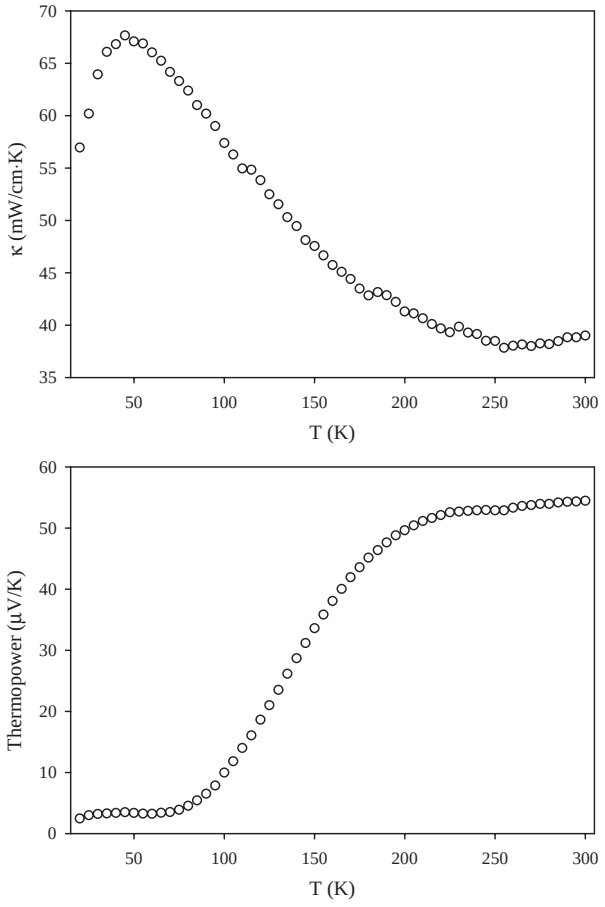

Fig. 5. Thermal conductivity and thermopower of $CrAuTe_4$ versus temperature.

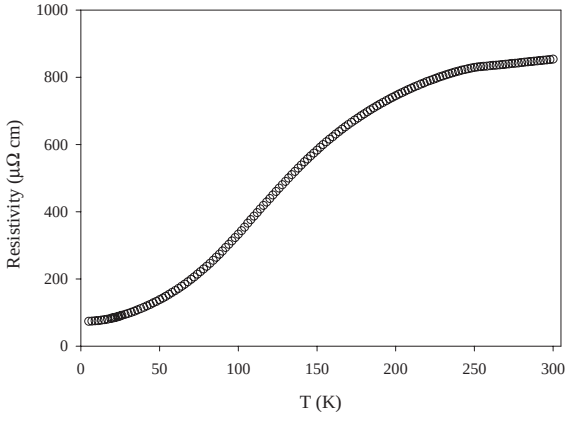

Fig. 6. Resistivity versus temperature for $CrAuTe_4$.

is typical for an extremely poor metal. This value decreases to about 75 $\mu\Omega \cdot$ cm at 5 K, which again is high for a metal. However, these values of resistivity are promising for thermoelectric materials. Unfortunately, the modest value of S in this temperature range makes this material unsuitable for thermoelectric applications.

Features in the resistivity and thermopower data are seen at about 255 K (see Fig. 7). As will be shown later,

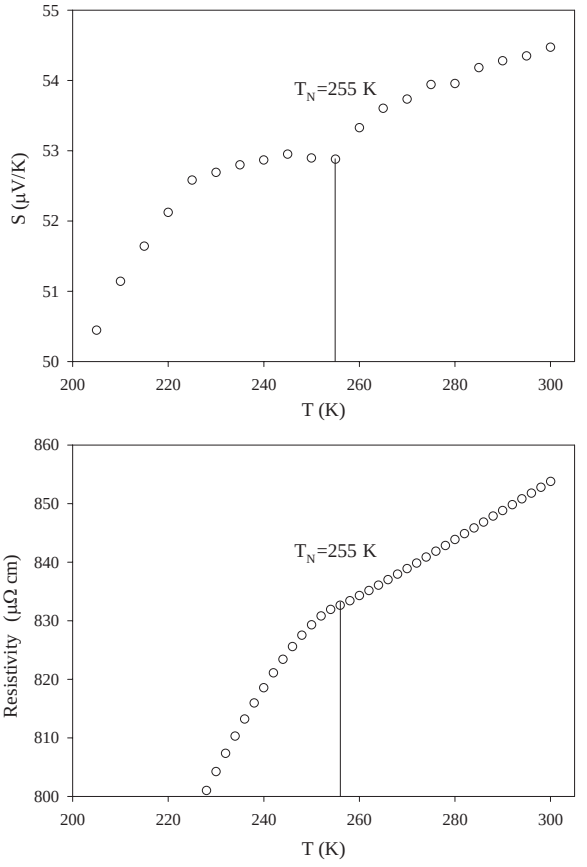

Fig. 7. Thermopower and resistivity versus temperature in the region of the antiferromagnetic phase transition at 255 K.

this temperature corresponds to an antiferromagnetic transition.

The thermal conductivity data presented in Fig. 5 has a typical shape for a pure (non-alloy) crystalline material. The thermal conductivity increases at low temperatures and then begins to decrease at about 50 K, indicating the onset of Umklapp scattering. Above this temperature a $1/T$ temperature dependence is observed. The thermal conductivity at room temperature is quite low, about 40 mW/cm K. However, this value is two to three times larger than the thermal conductivity of optimally doped Bi_2Te_3 alloys.

ZT as a function of temperature is plotted in Fig. 8 and at room temperature has a value of 0.027. Clearly, this is much lower than desired for thermoelectric materials.

3.3. Magnetic properties

The molar magnetic susceptibility, χ, is shown in Fig. 9. This figure shows that at 255 K $CrAuTe_4$ undergoes a paramagnetic to antiferromagnetic transition. While the resistivity and Seebeck coefficient are continuous through the transition, their first temperature derivatives show

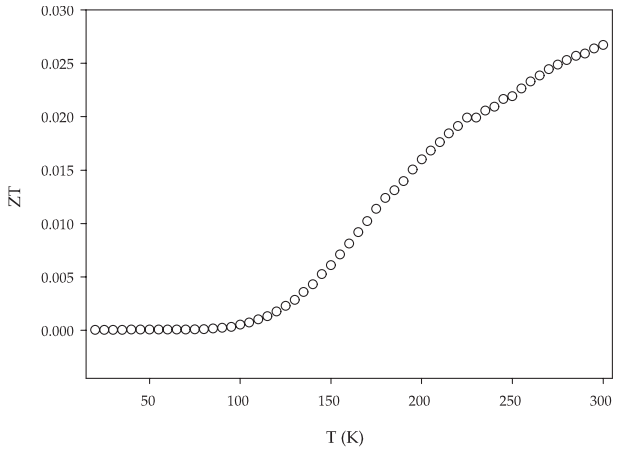

Fig. 8. ZT as a function of temperature for $CrAuTe_4$.

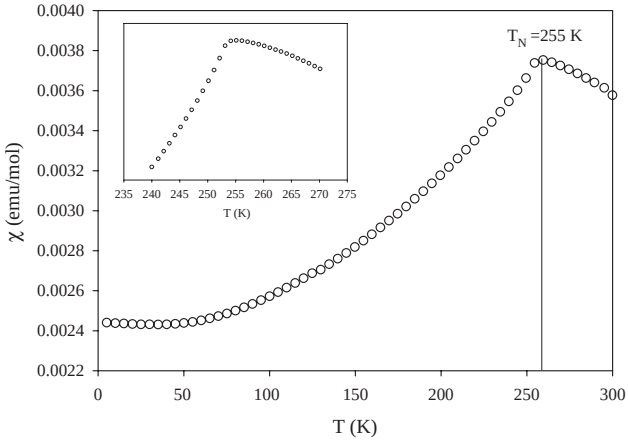

Fig. 9. Molar magnetic susceptibility versus temperature for $CrAuTe_4$. An antiferromagnetic phase transition occurs at 255 K.

obvious anomalies (Fig. 7). This is consistent with a second-order phase transition [23].

Magnetic-phase transitions are common in binary chromium tellurides. CrTe, Cr_5Te_6, and Cr_3Te_4 undergo complex magnetic-phase transitions at 125, 102, and 85 K, respectively [24]. Each appears to have several transitions as the material is cooled below 350 K [24]. Interestingly, these binaries are also ferro- or ferrimagnetic above room temperature [24].

The transition to antiferromagnetic ordering is attributed to the spins on the chromium cations since the calculated effective magnetic moment (μ_{eff}) is near 3.9 Bohr magnetons. Determination of μ_{eff} from the data begins with the Curie–Weiss law, given in Eq. (1).

$$\chi = \frac{C}{T+\theta}. \tag{1}$$

The value of θ is obtained from the paramagnetic portion of the curve. Typically θ is 1–4 times the Néel temperature, but would be equal to T_N in the molecular field theory for antiferromagnetism within the nearest neighbor approximation [25,26]. As a first approximation then we set $\theta = T_N$ and at the Néel temperature Eq. (1) can be written as

$$\chi = \frac{C}{2T_N}. \tag{2}$$

From the measured data T_N is 255 K, and χ is 0.003756 emu/mol at the Néel temperature. Therefore, C is equal to 1.916 emu K/mol. The effective paramagnetic moment, μ_{eff}, can be calculated from Eq. (3) [26].

$$\mu_{eff} = \left(\frac{3k_bC}{N_A}\right)^{\frac{1}{2}}. \tag{3}$$

Here, k_b is the Boltzmann constant, N_A is Avogadro's number, and C is the molar Curie constant.

From Eq. (3), the calculated effective magnetic moment per Cr atom is 3.91 μ_B. The expected effective magnetic moment of a Cr^{3+} ion is 3.87 μ_B (for $g = 2$ and $S = \frac{3}{2}$), and thus the magnetic ordering in the compound is ascribed solely to antiferromagnetic interactions between the Cr^{3+} ions.

The molecular field theory in the nearest neighbor approximation can also be used as a model for the susceptibility below T_N. In this model, the ratio of the susceptibility at the Néel temperature to that at 0 K should be $\frac{3}{2}$ [25]. The measured susceptibility of $CrAuTe_4$ is 0.00374 emu/mol at T_N and can be extrapolated to 0.00243 emu/mol at 0 K. Thus the ratio of the susceptibility at the Néel temperature to the susceptibility at 0 K is 1.53, which agrees well with the expected value of $\frac{3}{2}$. If the Cr is formally 3+, then the Au would also be 3+. It is not surprising that square planar d^8 Au(III) is non-magnetic ($S = 0$).

4. Conclusion

A new ternary gold telluride has been synthesized and has structural characteristics similar to that of the binary $AuTe_2$. It is one of only a few-known ternary gold tellurides. Most known polytellurides are alkali metal compounds and are Zintl phases. In this case, besides tellurium, the only atoms present are transition metals. There is direct Te–Te bonding and formal oxidation states can be assigned as $Cr^{3+}Au^{3+}(Te_2)^{2-}Te_2^{2-}$. This compound may therefore be considered a ternary transition metal Zintl phase.

Through magnetic susceptibility measurements, chromium has been shown to be in the +3 oxidation state. The effective magnetic moment per chromium cation agrees well with the theoretically expected value. To achieve charge balance in the compound, the Au oxidation state must be also +3 as noted above. Au adopts a square planar coordination geometry which is very typical for d^8 configurations and results in $S_{Au} = 0$.

Transport measurements were carried out to determine the thermoelectric properties of this material. The small values of the thermopower make it unsuitable for thermoelectric applications. At room temperature, the thermopower is about four times smaller than that of optimally doped Bi_2Te_3 alloys.

Acknowledgments

This work was funded by NSF Grant # DMR-0115732. We thank Dr. Emil B. Lobkovsky for assistance in collecting single crystal data. We also thank John Hunt for guidance in using the electron microprobe facility in the Cornell Center for Materials Research which is supported through a MRSEC Grant (DMR-0079992). TKR also thanks the American Society for Engineering Education for support through a National Defense Science and Engineering Graduate Fellowship (NDSEG).

References

[1] S. Sinani, G. Gordyakova, Sov. Phys.-Tech. Phys. 1 (1957) 2318–2319.
[2] H. Benel, Compt. Rend. 247 (1958) 584–587.
[3] U. Birkholz, Z. Naturforsch. 13a (1958) 780–792.
[4] K. Smirous, L. Stourac, Z. Naturforsch. 14a (1959) 848–849.
[5] S. Airapetyants, B. Efimova, T. Stavitskaya, L. Stilbans, L. Sysoeva, Soviet Phys.-Tech. Phys. 2 (1957) 2009–2011.
[6] E. Elagina, N. Abrikosov, Zh. Neorg. Khim. 4 (1959) 1638–1642.
[7] H. Goldsmid, J. Appl. Phys. 32 (1961) 2198–2202.
[8] A. Rosenberg, A. Strauss, Phys. Chem. Solids 19 (1961) 105–116.
[9] F. DiSalvo, Science 285 (5428) (1999) 703–706.
[10] P. Messien, M. Baiwir, Bull. Soc. Roy. Sci. Lieg. 35 (1966) 234–243.
[11] G. Tunell, L. Pauling, Acta Crystallogr. 5 (1952) 375–381.
[12] W. Bronger, H. Kathage, J. Alloys Compounds 184 (1992) 87–94.
[13] SMART and SAINT: Data collection and processing software for the SMART system, Bruker Analytical X-ray Instruments, Inc., Madison, WI, 1995.
[14] X-SHAPE version 1.01 program for absorption correction, STOE and Cie GmbH Darmstadt, 1996.
[15] XPREP program for determination of space groups, Bruker Analytical X-ray Instruments, Inc., Madison, WI, 1996.
[16] G.M. Sheldrick, SHELXTL version 5.1, for Bruker Analytical X-ray Instruments, Inc., Madison, WI, 1996.
[17] A. Altomare, G. Cascarano, C. Giacovazzo, A. Guagliardi, Appl. Crystallogr. 26 (1993) 343–350.
[18] L. Farrugia, J. Appl. Crystallogr. 32 (1999) 837–838.
[19] R. Taylor, Measurement of thermal properties, in: CRC Handbook of Thermoelectrics, CRC Press, Boca Raton, FL, 1995, pp. 165–180.
[20] H. Swanson, E. Tatge, Nat. Bureau Stand. (US) 359 (1953) 1–95.
[21] P. Boettcher, J. Getzschmann, R. Keller, Z. Anorg. Allg. Chem. 619 (1993) 476–478.
[22] W. Schutte, J. de Boer, Acta Crystallogr. B 44 (1988) 486–494.
[23] R. White, T. Geballe, Long Range Order in Solids, Academic Press, New York, 1979.
[24] T. Koneshova, K. Eremin, V. Novotvortsev, Inorg. Mater. 31 (12) (1995) 1385–1388.
[25] B. Cullity, Introduction to Magnetic Materials, Addison-Wesley, Reading, MA, 1972.
[26] J. Smart, Effective Field Theories of Magnetism, W.B. Saunders Co., London, 1966.